Geoscience Frontiers 13 (2022) 101324

Contents lists available at ScienceDirect

Geoscience Frontiers

journal homepage: www.elsevier.com/locate/gsf

Research Paper

Paleo-oil reservoir pyrolysis and gas release in the Yangtze Block imply an alternative mechanism for the Late Permian Crisis

Chengyu Yang [a], Meijun Li [a,b,*], Zhiyong Ni [a], Tieguan Wang [a], Nansheng Qiu [a], Ronghui Fang [c,d], Long Wen [e]

[a] State Key Laboratory of Petroleum Resources and Prospecting, China University of Petroleum (Beijing), College of Geosciences, China University of Petroleum (Beijing), Beijing 102249, China
[b] Key Laboratory of Exploration Technologies for Oil and Gas Resources (Yangtze University), Ministry of Education, College of Resources and Environment, Yangtze University, Wuhan, Hubei 430100, China
[c] Oil & Gas Survey, China Geological Survey, Beijing 100083, China
[d] The Key Laboratory of Unconventional Petroleum Geology, China Geological Survey, Beijing 100083, China
[e] Exploration and Development Research Institute of Southwest Oil & Gas Field Company, PetroChina, Chengdu, Sichuan 610041, China

ARTICLE INFO

Article history:
Received 4 March 2021
Revised 8 October 2021
Accepted 29 October 2021
Available online 1 November 2021
Handling Editor: R.D. Nance

Keywords:
Oil reservoir pyrolysis
Hydrothermal fluid
Emeishan Large Igneous Province
Gas release
Mass extinction

ABSTRACT

The causes of the global mass extinction that occurred around the Permian–Triassic boundary have been widely studied through the geological record and in various locations. The results show that volcanic activity was a key factor in initiating the crisis during the Late Permian. Compared to other thermal events triggered by volcanic activity, pyrolysis of petroleum in Pre-Permian reservoirs has rarely been suggested as a significant source of the greenhouse gases that caused the mass extinction. In this study, geochemical analysis is carried out of a huge paleo-oil reservoir in the Yangtze Block (YB), South China. The detection of mineral inclusions and pyrobitumens is evidence of rapid pyrolysis of accumulated oil in the Ediacaran reservoir. New evidence from hydrothermal minerals and the presence of domain mesophase in the pyrobitumen suggest that the pyrolysis process occurred abruptly and that greenhouse gases were rapidly released through venting pipes. The dating of such a complex geological event in this old and deeply buried reservoir is inevitably difficult and potentially unreliable. However, cross-validation of the multiple evidence sources, including hydrothermal minerals and domain mesophase, indicates that the rapid oil pyrolysis must have been driven by a major thermal event. Reconstruction of burial and thermal histories suggests that the thermal event was most likely to have been triggered by the Emeishan Large Igneous Province (ELIP), which was in a period of significant volcanic activity during the Late Permian. Massive volumes of gases, including methane, carbon dioxide, and possibly hydrogen sulfide, were released, causing a significant increase in greenhouse gases that may have contributed to global warming and the resulting mass extinction during the Late Permian Crisis (LPC).

© 2021 China University of Geosciences (Beijing) and Peking University. Production and hosting by Elsevier B.V. This is an open access article under the CC BY-NC-ND license (http://creativecommons.org/licenses/by-nc-nd/4.0/).

1. Introduction

Thermal alteration of petroleum is a disproportionate reaction involving a range of reactions among different types of organic matter (Horsfield et al., 1992; Geng and Liao, 2002; Ding et al., 2013; Lorant et al., 2000), and producing gas and solid bitumen in deeply buried hydrocarbon reservoirs (Milner et al., 1977; Yang et al., 2018a). Solid bitumen can be created by many processes, including thermal alteration of overmature source rock, which is common in reservoirs and late oil windows (Jacob, 1989; Rippen et al., 2013; Mastalerz et al., 2018; Sanei, 2020). Highly mature solid bitumen is usually called pyrobitumen and is characterized by its low solubility and the occurrence of mesophase, which denotes graphitization of petroleum in reservoirs and source rocks (Mastalerz et al., 2018; Yang et al, 2018a). The ceiling temperature for petroleum pyrolysis under geological conditions is 200 °C (Waples, 2000; Spigolon et al., 2015). Further heating might cause polycondensation reactions, generating polycyclic aromatic hydrocarbons (PAHs) as precursors of mesophase (Lewis and Kovac, 1978, 1980, 1987; Forrest and Marsh, 1983; Goodarzi, 1984; Mochida, et al., 1984). Crystallization and graphitization under higher temperatures would finally transform the mesophase into graphite (White and Price, 1974; Goodarzi and Norford, 1985; Jacob, 1989). A temperature of over 350 °C is needed to maintain a pyrolysis-polycondensation reaction under

* Corresponding author.
E-mail addresses: meijunli@cup.edu.cn, meijunli2008@hotmail.com (M. Li).

https://doi.org/10.1016/j.gsf.2021.101324
1674-9871/© 2021 China University of Geosciences (Beijing) and Peking University. Production and hosting by Elsevier B.V.
This is an open access article under the CC BY-NC-ND license (http://creativecommons.org/licenses/by-nc-nd/4.0/).

experimental conditions because, under high temperatures, PAHs remain liquid, which allows the upgrading of mesophase (White and Price, 1974; Lewis and Kovac, 1978; Tian, 2013). The generation of mesophase pitch in geological conditions indicates intensive pyrolysis and devolatilization of oil under high temperature, which could generate huge upward pressure against overlying strata (Barker, 1990; Svensen et al., 2009; Yang et al., 2018b). The accumulated pressure could be greater than 200 MPa, probably enough to cause fracturing (Yang et al., 2018b). Gas venting pipes created by the fracturing could release large volumes of natural gases into the air, which may have contributed to global warming and mass extinctions in geological history (Svensen et al., 2009).

The Late Permian Crisis (LPC) is the most severe mass extinction in Earth's history. Two independent extinction events occurred within a relatively short period (less than 10 Myr); the Guadalupian-Lopingian Extinction (GLE) (Stanley and Yang, 1994; Jin et al., 1998; Kirschvink et al., 2015) and the Permian–Triassic Extinction (PTE) (Knoll et al., 2007; Penn et al., 2018; Grasby et al., 2020). Previous studies have suggested that these extinctions could have been triggered by volcanic activity (for instance in the Siberian Traps) (Wignall, 2001; Black et al., 2012; Burgess et al., 2017), oceanic anoxia (Clapham and Payne, 2011; Zhang et al., 2018), strongly fluctuating ocean redox conditions (Elrick et al., 2017), wildfires (Hudspith et al., 2014; Vajda et al., 2020), organic matter combustion (Grasby et al., 2011; Elkins-Tanton et al., 2020), and possibly extraterrestrial impacts (Becker et al., 2001; Tetsuji et al., 2019). Any of these events could have resulted in abrupt climate change, such as massive global warming, which could have rapidly exterminated Earth's existing biomass and led to a comparatively lifeless period (Roscher et al., 2011; Cui and Kump, 2014). Gas hydrates, ocean sediments, and volcanism are all considered to be potential sources of greenhouse gases (Ganino and Arndt, 2009; Clarkson et al., 2015; Jerram et al., 2015). Natural gases from the thermal decomposition of dolomite, evaporite, coal, or organic-rich shale may have also contributed to the LPC (Stanley and Yang, 1994; Ganino and Arndt, 2009; Svensen et al., 2009; Grasby et al., 2011; Elkins-Tanton et al., 2020; Grasby et al., 2020).

Pyrolysis of paleo-oil reservoirs is common in the southern YB and other locations around the world (Shi et al., 2015). However, few studies have looked at the influence of pyrolysis on the paleo-environment. Many large paleo-oil reservoirs are currently covered by thick overlying strata, so it is difficult to reconstruct the process of pyrolysis in detail. The relationship between thermal events and paleo-oil pyrolysis is also difficult to establish from the organic matter and authigenic minerals in reservoirs because these materials will have been transformed by long-term burial, which is likely to have overprinted information from previous thermal events.

After many years of research on petroleum systems in the Chuanzhong Uplift, numerous studies on pyrobitumen (Yang et al., 2018a), methane inclusions in dolostone gas reservoirs (Yang et al., 2018b), burial and heat histories (Zhu et al., 2016; Liu et al., 2018), and seismic data (Yang et al., 2017) have all implied that an enormous paleo-oil reservoir of Ediacaran dolostone in the YB (a historical oil reservoir which transformed to a gas reservoir) was rapidly pyrolyzed by a hydrothermal fluid invasion under high temperature conditions (over 300 °C) (Yang et al., 2018a,b). In this study, new data from hydrothermal minerals and highly graphitized pyrobitumen suggest a model of oil pyrolysis and gas release in the Ediacaran reservoir that might be directly related to the Late Permian Crisis, although it is impossible to accurately determine the timing of the pyrolysis. For the first time, the results of this research reveal a model for pyrolysis and gas release in a paleo-oil reservoir. This new topic may shed light on the evolution of the thermal-related paleo-oil reservoirs that are currently being discovered. It may be that underground petroleum made a significant contribution to climate change and mass extinctions in geological history in addition to the more obvious contributions of surface organic matter.

2. Geological settings

The Anyue giant gas fields was discovered in 2011 in the Chuanzhong Uplift in the western part of the Yangtze Block (Fig. 1a). Natural gas had accumulated in Ediacaran carbonate sediments, which lie on a pre-Ediacaran crystalline basement (Jiang et al., 2014). The confirmed source rocks are black shales of the Lower Cambrian Qiongzhusi Formation ($\epsilon_1 q$) (Zou et al., 2014) (Fig. 1b). The most productive Ediacaran reservoirs include the Dengying-2 and Dengying-4 formations (Z_2dn2 & Z_2dn4), which are separated by the thin shale of the Dengying-3 Formation (Z_2dn3) (Fig. 1b). Thick dolostone formations in the Cambrian include the Gaotai and Longwangmiao formation ($\epsilon_1 g$ & $\epsilon_1 l$) which overlie the $\epsilon_1 q$ source rocks. The Z_2dn2 & Z_2dn4 formations are mostly composed of algal reef, while $\epsilon_1 g$ & $\epsilon_1 l$ consist of grain dolostone and mud dolostone (Zhu et al., 2015). The gas fields are thought to have been generated by *in situ* pyrolysis of a huge paleo-oil reservoir (Zhu et al., 2015; Gao et al., 2018; Yang et al., 2018a,b). Pyrobitumens have been widely and continuously discovered in the Chuanzhong Uplift, an anticline structure formerly called the Leshan-Longnvsi Uplift (Zhu et al., 2015; Yang et al., 2018a). The main body of the paleo-oil reservoir may therefore be in this uplift. (Fig. 1a). Conservative estimates suggest that the current reserves of natural gas in the field are 7×10^{11} m^3 (0.5×10^{15} g) (Zhu et al., 2015). The natural gas is typical dry gas, consisting of more than 95% CH_4, with small amounts of H_2S, CO_2, N_2, and He (Zhu et al., 2015).

A magmatic plume of predominantly basaltic composition occurred during the convergence of Pangaea (Fig. 1a), intruding into the southwest of the YB (Chung and Jahn, 1995; Wignall et al., 2009; Jerram et al., 2015). This plume is generally known as the Emeishan Large Igneous Province (ELIP), or Emeishan Traps. The ELIP covers an area of at least 2.5×10^5 km^2 in the western margin of the Sichuan Basin, and is also likely to be present, but concealed, in the center part of the basin (He et al., 2003). The most recent exploration well in this region (YS1) (Fig. 1a), drilled by the China National Petroleum Corporation (CNPC), discovered a gas reservoir in igneous rock in the Upper Permian, which tends to confirm the presence of branches of the ELIP in the center of the basin (Wen et al., 2019). Well data and seismic interpretation indicate that the ELIP is geographically adjacent to the gas field in the center of the Sichuan Basin and may have had a significant impact on the evolution of the Ediacaran petroleum system (Gao et al., 2018; Liu et al., 2018; Yang et al., 2018a).

3. Samples and methods

Carbonate samples were collected from well cores drilled in the Chuanzhong Uplift, from the Ediacaran to the lower Cambrian successions (Fig. 1c). The samples were polished to approximately 0.03 mm thickness and used in both cross-polarization microscopy and cathodoluminescence (CL) microscopy. Microscopic observation of sections was performed using a Leica DM4000 microscope. The pyrobitumen samples were molded using epoxy resin and polished, according to the standard method ASTM (No. D7708-14), in the State Key Laboratory of Petroleum Resources and Prospecting, China University of Petroleum (Beijing). Optical study of the samples was carried out using a Leica DM4500P microscope with an oil-immersion objective using reflected light. Measurement of % BR_o (bitumen reflectance with oil-immersion objective) was performed at 546 nm wavelength (1.518 refractive index oil) using a

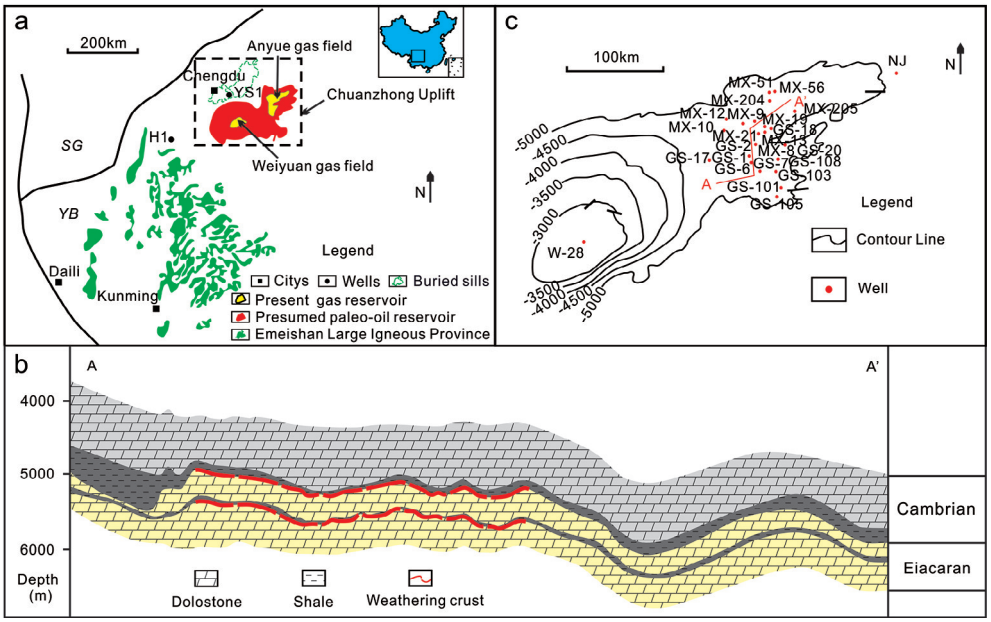

Fig. 1. Generalized geological map showing the location and area of the Emeishan Large Igneous Province, including the gas fields: (a) Stratigraphic section of the main body of the Anyue gas field (after Yang et al., 2018a); (b) the structural characteristics and sampled wells on the Chuanzhong Uplift: (c) (SG = Songpan-Ganze accretionary complex; YB = Yangtze Block);

CRAIC Microscope photometer (with a measuring spot area of 1 μm^2). The anisotropic pyrobitumen sample was rotated under polarized light, and averages of $\%BR_{omax}$ were recorded for each sample.

A Scanning Electron Microscope-Energy Dispersive Spectrometer (SEM-EDS) was used to observe the morphology and determine the element composition of the pyrobitumen. Pyrobitumen samples were separated from the dolostone by acid dissolution. Immersion in diluted hydrochloric acid at 35 °C for 10 h was used to dissolve dolostone fragments approximately 1 cm in diameter. Immersion in hydrofluoric acid at 25 °C for 5 h was then used to dissolve the silicate. The pyrobitumen pieces were collected from the residue of the acid treatment, coated with gold, and analyzed on Quanta200F and Hitachi SU8010 field emission SEM-EDSs.

A total of eighteen rock samples were ground to finer than 200 mesh powder using an agate mortar & pestle and then prepared for stable carbon and oxygen isotope analysis (Table 1). Before they were powdered, the samples were all observed by microscope to identify the principal dolomite type (Table 1). Powder from each sample was then reacted with 100% phosphoric acid in a dissolving device. The resulting CO_2 gas was analyzed using a MAT253 mass spectrometer to measure carbon and oxygen isotope values. Both carbon and oxygen isotope values were reported in pairs per thousand relative to Vienna Peedee Belemnite (VPDB). Analytical errors were generally within 0.01‰. All the samples were analyzed in the State Key Laboratory of Petroleum Resources and Prospecting, China University of Petroleum, Beijing.

4. Results

4.1. Hydrothermal minerals in reservoirs

The Ediacaran dolostone reservoirs are mainly composed of algal reef (Zhu et al., 2015) (Fig. 2a, b). The unconformity at the

Table 1
Carbon and oxygen isotopes of the Ediacaran dolostone samples.

Well	Depth (m)	Lithofacies	Crystal size	$\delta^{18}O_{VPDB}$ (‰)	$\delta^{13}C_{VPDB}$ (‰)
GS18	5208.2	Fine grain dolostone	Cryptocrystalline	−3.93	0.77
MX13	5104.7	Algal dolostone		−4.74	3.33
MX21	5139.4	Algal dolostone		−4.77	2.72
MX51	5396.6	Algal dolostone		−3.12	3.25
GS2	5393	Fine grain dolostone	Crystalline	−6.69	0.64
MX10	5471.1	Fine grain dolostone		−7.86	0.79
GS20	5253.8	Algal dolostone		−6.22	2.74
GS7	5327.5	Algal dolostone		−7.78	3.26
MX9	5424.3	Fine grain dolostone		−6.74	0.76
GS2	5015.2	Mud-dolostone		−6.25	1.66
MX9	5033.6	Mud-dolostone		−6.30	1.92
MX8	5425.2	Fine grain dolostone		−9.13	1.30
GS103	5291.0	Mud-dolostone		−8.14	1.89
GS101	5498.8	Mud-dolostone		−8.32	2.13
GS103	5291.4	Algal dolostone	Saddle	−11.12	−0.69
GS105	5220	Algal dolostone		−11.81	3.05
GS103	5177.4	Algal dolostone		−11.61	1.39
GS101	5517.5	Algal dolostone		−11.37	0.39

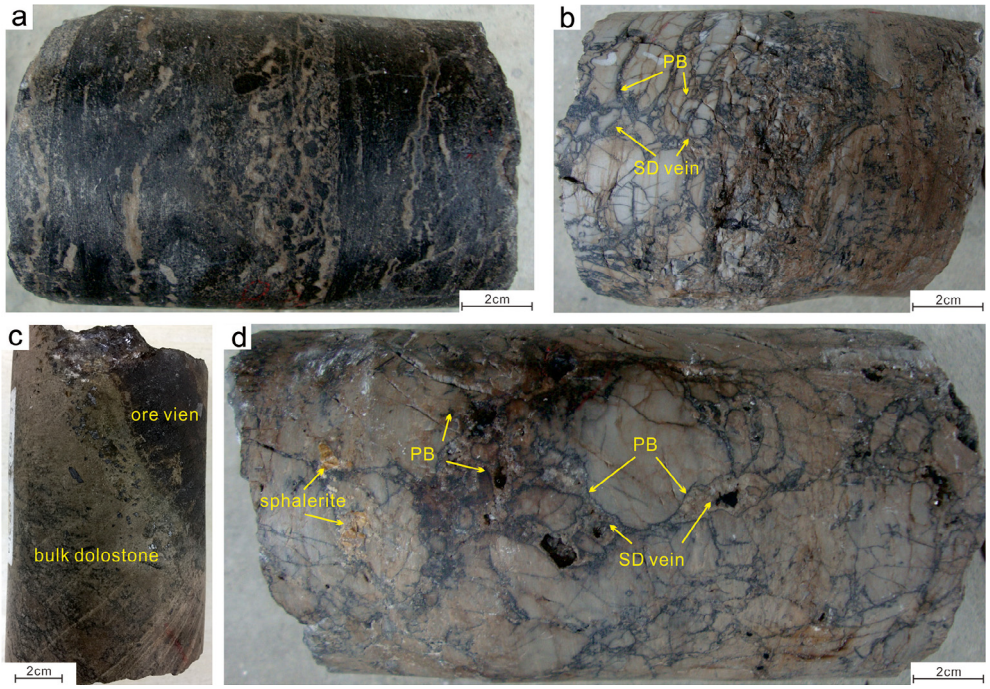

Fig. 2. Images of the core samples, PB = pyrobitumen, SD = saddle dolomite: (a) core of Ediacaran algal dolostone, Well MX10, 5382 m; (b) cracking micrite dolostone coated with pyrobitumen film, and then cemented by saddle dolomite vein, Well GS108, 5274 m; (c) hydrothermal mineral vein, Well GS101, 5177 m; (d) cracking micrite dolostone coated with pyrobitumen film and then cemented by saddle dolomite vein with hydrothermal minerals, Well GS108, 5277 m.

top of the Ediacaran succession points to strong meteoric karstification (Fig. 2b) which occurred at the end of the Ediacaran period (Wei et al., 2013; Zou et al., 2014; Zhu et al., 2015). Caves and cracks were created by the karstification and filled with vein minerals including quartz, metal sulfide (including sphalerite and galena) (Fig. 2c), dolomite of different generations, and pyrobitumen (Fig. 2d).

Ediacaran dolostone can be divided into three types: micritic dolomite, spar dolomite, and saddle (baroque) dolomite (Gregg and Karakus, 1991; Feng et al., 2017; Hu et al., 2020). Micritic dolomite is the principal component of the dolostone skeleton and includes algae, grains, and several early cements (Fig. 3a). Typically, micritic dolomite is dim under a CL microscope (Pierson, 1981; Fairchild, 1983; Machel, 1985) (Fig. 3c). Spar dolomite commonly forms with a cloudy center and a clear rim (Fig. 3b) and exhibits internal zonation under a CL microscope (Fig. 3c). Saddle dolomite always fills in the centers of pores alongside vein minerals including quartz, sphalerite, and galena, as well as pyrobitumen

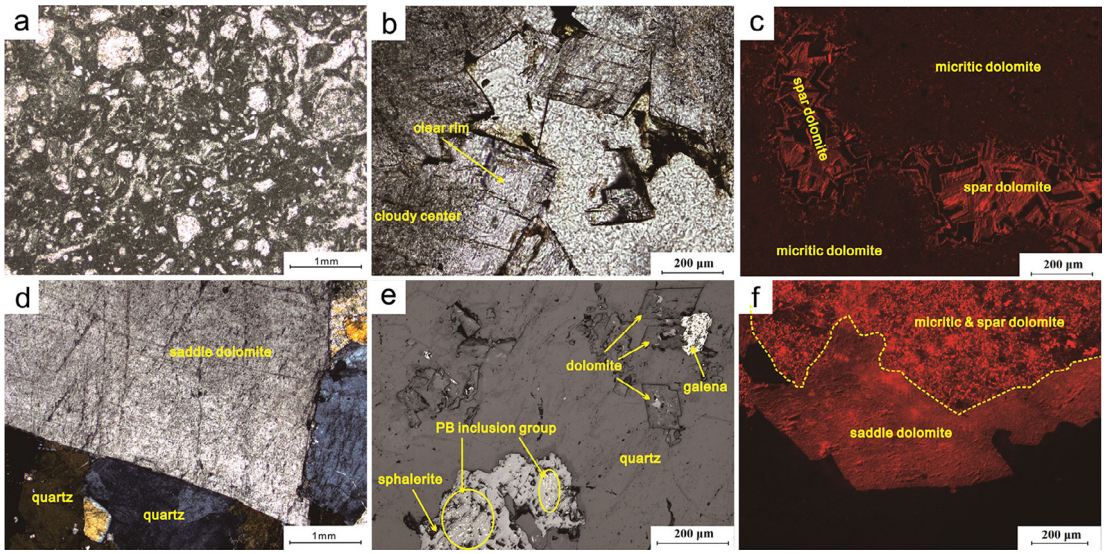

Fig. 3. Photomicrograph of petrology characteristics and diagenesis of the samples: P = plane-polarized transmission light, C = cross-polarized transmission light, CL = cathode luminescence, PRF = plane-polarized reflected light. (a) Algal dolostone with algal and spicular clastic grain, Well GS108, 5248 m, (P); (b) spar dolomite with cloudy center and clear rim, Well GS105, 5220 m, (P); (c) micritic dolomite and spar dolomite in dolostone, Well GS108, 5248 m, (CL); (d) saddle dolomite with quartz in veins, Well GS103, 5177 m, (C); (e) minerals in a hydrothermal mineral vein, Well GS101, 5177 m, (PRF); (f) saddle dolomite and indistinguishable micritic dolomite and crystal dolomite, Well MX19, 5438 m, (CL).

(Fig. 3d, e), but does not exhibit any internal zonation in CL photomicrographs (Fig. 3f).

The isotopic values of dolomite samples were divided into three groups according to their types (Fig. 4). The $\delta^{13}C$ values of all dolomites are mainly positive, ranging from −0.69‰ to +3.33‰ (Table 1). The differences in the $\delta^{13}C$ values between the three types of dolomites are insignificant. The saddle vein material dolomite shows the lowest $\delta^{18}O$ value (Fig. 4), ranging from −11.12‰ to −11.81‰ (Table 1). Optical observation reveals that the fracture-filled dolomite is almost saddle dolomite (Table. 1), while the fact that the saddle dolomite has the lowest $\delta^{18}O$ value implies that it was formed by hydrothermal fluids (Warren, 2000; Loyd et al., 2015; Feng et al., 2017).

The $\delta^{18}O$ values of crystalline and cryptocrystalline dolomite represent spar dolomite and micritic dolomite, respectively, under optical observation (Table 1). The spar dolomite has a lower $\delta^{18}O$ value than the micritic dolomite, showing that the $\delta^{18}O$ values of dolomites decrease with diagenetic evolution in the reservoir (Fig. 4).

4.2. Graphitizing pyrobitumen

Pyrobitumen is a by-product of oil cracking in reservoirs, and its occurrence is strong evidence of a heated paleo-oil reservoir. The discovery of mesophase in the pyrobitumen in the samples indicates that the oil was pyrolyzed at a temperature of at least 350 °C (White, 1976; Goodarzi, 1984; Goodarzi and Norford, 1985; Teichmüller, 1986; Yang et al., 2018a). The enhancement of the optical texture of the mesophase, from matrix to grain flow, and domain, indicates its graphitizing class (White, 1976; Yang et al., 2018a). Graphitization begins at the primary stage and gradually progresses through low, medium, and high classes. High class mesophase is composed of intensively layered mesophase lamellae (White, 1976; Yang et al., 2018a) and usually has a flow-domain texture, depending on the architecture of the lamella-forming morphology (White, 1976; Ragan and Marsh, 1981; Yang et al., 2018a). Occurrence of domain mesophase in pyrobitumen is commonly considered to be a mark of natural oil pyrolysis (Brooks and Taylor, 1965; Yang et al., 2018a). Observation shows that domain mesophase is common in the Ediacaran reservoir (Fig. 5). Flow-domain texture is observable under reflected light (Fig. 5a, b). SEM images show that the mesophase lamellae are closely packed, similar to the morphology of graphite (Goodarzi, 1984; Goodarzi and Norford, 1985; Teichmüller, 1986) (Fig. 5c, d).

SEM images of the pyrobitumen show evident molds of escaped bubbles on the convex surfaces of pure pyrobitumen pieces, while moulage of pressed bubbles is observed on concave surfaces (Fig. 6). The pyrobitumen must have been liquid when the gas bubbles formed, so the reservoir temperature at that time was higher than 300 °C. The molds and moulage could then have been created by the low-boiling composition (White, 1976; Yang et al., 2018a).

4.3. Migration route of the hydrothermal fluid

Saddle dolomite is considered to be a consequence of hydrothermal dolomitization (Braithwaite and Rizzi, 1997; Davies and Smith, 2006) and commonly occurs alongside galena, sphalerite and quartz (Fig. 7a, b, c). These minerals frequently coeval with MVT (Mississippi Valley-type) lead–zinc deposits (Basuki and Spooner, 2004; Leach et al., 2005, 2010; Davies and Smith, 2006; Paradis et al., 2007). MVT lead–zinc deposits always occur in the form of late-stage veins or pore fillings, evidence that epithermal solutions invaded the reservoir (Fig. 3) (Jiang et al., 2016; Yang et al., 2018a,b). Pyrobitumen associated with the MVT lead–zinc deposits filled the pores of the reservoir rocks (Fig. 7d) (Yang et al., 2018a,b). Studies have confirmed that the Ediacaran dolostone underwent two periods of karstification, which formed the weathering crust on the tops of the Z_2dn2 and Z_2dn4 formations (Wei et al., 2013; Zou et al., 2014; Zhu et al., 2015) (Fig. 1b). The karstification created most of the pore space, including vugs and cracks (Fig. 2c, d) under the weathering crust, and turned the dolostone into a high-quality reservoir (Wei et al., 2013; Zou et al., 2014; Zhu et al., 2015). The weathering crust and cracks in the reservoir would have provided a perfect path for the hydrothermal fluid intrusions that precipitated most of the saddle dolomite (Jiang et al., 2016; Yang et al., 2018a).

The MVT lead–zinc vein is mainly found in the wells of the southwest of the Anyue gas field, including GS-105. GS-101, GS-

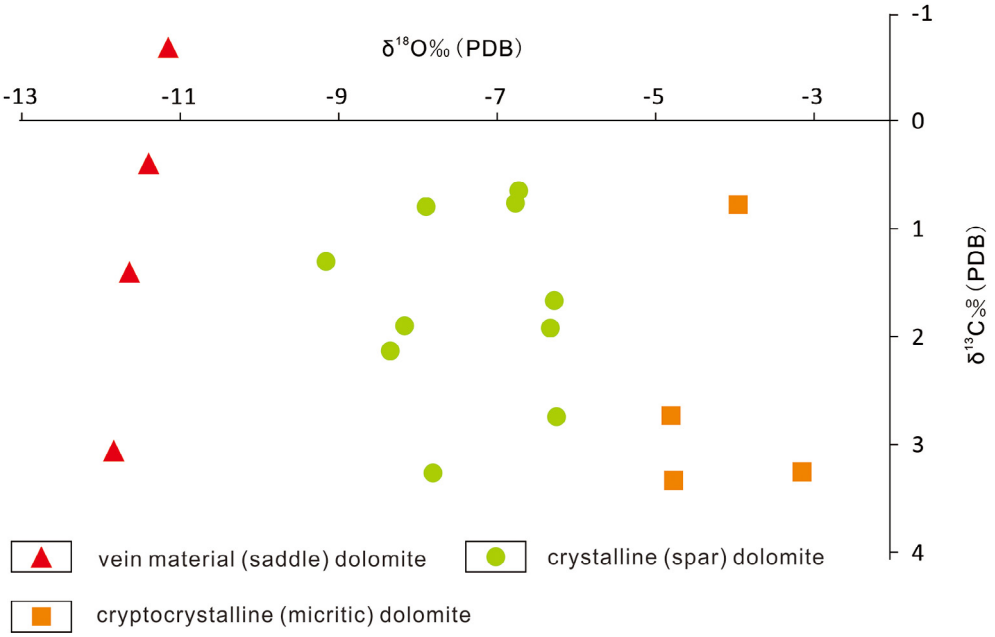

Fig. 4. Cross-plot of stable carbon and oxygen isotopes of Ediacaran dolostone.

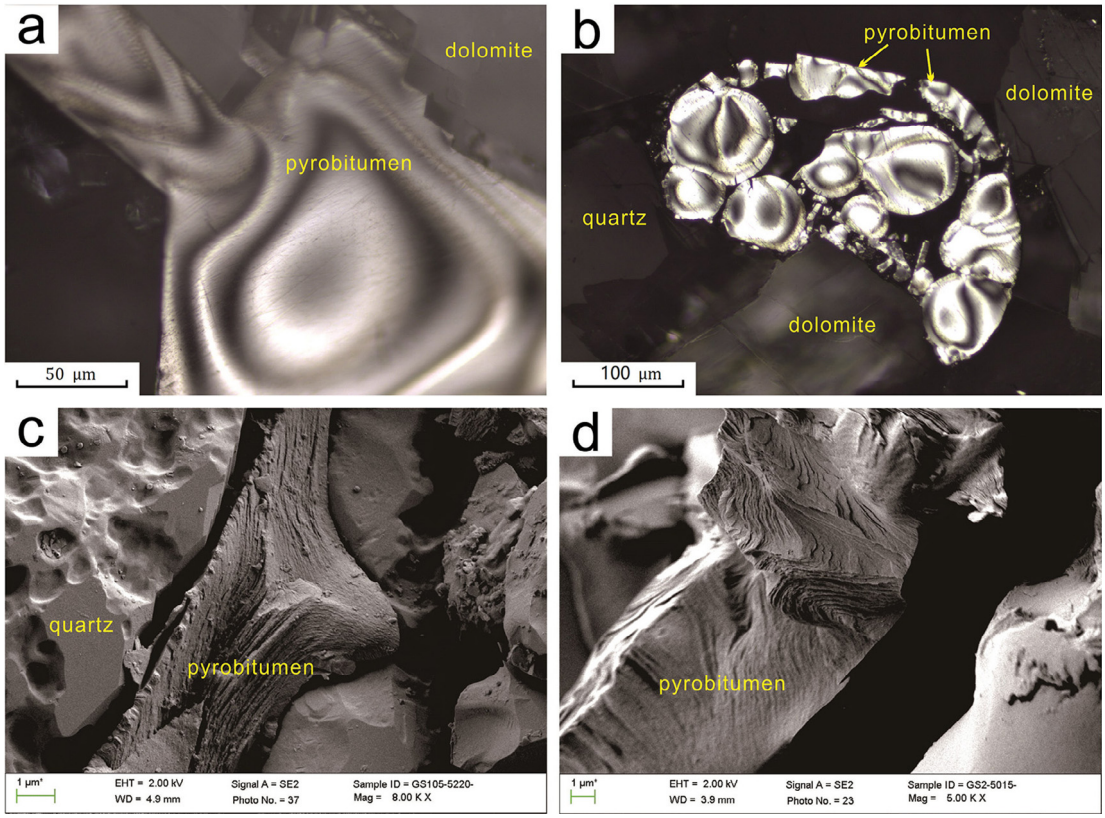

Fig. 5. Photomicrographs of high maturity grade pyrobitumen in the dolostone reservoir. PRF = plane-polarized reflected light, SEM = scanning electron microscope image. (a) Pyrobitumen with a flow-domain texture (PRF), Well GS105, 5220 m; (b) high maturity grade pyrobitumen in a group of pores of the dolostone reservoir (PRF), Well GS7, 5328 m; (c) high maturity grade pyrobitumen in a crack in quartz (SEM), Well GS105, 5220 m; (d) section of flow-domain mesophase in high maturity grade pyrobitumen (SEM), Well GS2, 5015 m.

1, GS-2 and GS-7 (Fig. 1c, 3, 7). Sphalerite and galena are found in hydrothermal veins in cores (Fig. 7a, b, c). However, the amounts of different kinds of hydrothermal minerals are not consistent in the Chuanzhong Uplift. Sphalerite and galena are rare in the northeast wells, and saddle dolomite is small and difficult to distinguish from spar dolomite (Table 1). These differences are also apparent in the successions in the Chuanzhong Uplift. Investigation confirms that typical lead–zinc deposits are more likely to occur in Ediacaran reservoirs than in Cambrian reservoirs (Figs. 7, 8). As the images show, the most common hydrothermal mineral in $\epsilon_1 l$ is illite (Fig. 8), implying a hydrothermal fluid temperature lower than 200 °C in the Cambrian reservoir. The illite in $\epsilon_1 l$ occurs as late-stage pore filling, always with pyrobitumens and in filiform shape, which means it was formed by hydrothermal fluid with a temperature below 200 °C (Chuhan et al., 2000; Pluijm et al., 2001; Rahl et al., 2011) (Fig. 8c).

The mesophase in pyrobitumen of different classes has a similar distribution to the hydrothermal fluid minerals. Mesophase is a mark of the final graphitization of organic matter under high temperature (Gentzis, and Goodarzi, 1993; Rimmer et al., 2015; Yang et al., 2018a). Domain mesophase (the same as sub-graphite) represents the final form of organic matter in the reservoir (Teichmüller, 1986; Jacob, 1989; Yang et al., 2018a). The micro-texture and $\%BR_{omax}$ of the pyrobitumen show that high class mesophase with domain and flow-domain optical textures is concentrated in the southwest of the Chuanzhong Uplift (GS wells) (Fig. 1c; Table 2). Moreover, the mesophase in the Ediacaran reservoir has an evidently higher micro-texture and $\%BR_{omax}$ than the mesophase in the Cambrian reservoir, because the micro-texture of the mesophase in the Cambrian reservoir is mainly grain, while it transformed into flow-domain in the Ediacaran reservoir (Table 2). The $\%BR_{omax}$ of the pyrobitumen in the southwest wells (GS wells) is generally between 5.92% and 7.49%, with an average of 7.03%, while in the northeast wells (MX wells) it is generally between 5.55% and 7.34%, with an average of 6.13% (Table 2).

5. Discussion

5.1. Pyrolysis of the oil

Studies have shown that, under quite high temperatures (350–600 °C, oil pitch transforms into a mixture of polycyclic aromatic hydrocarbons and other derivatives through pyrolysis and condensation reactions (White, 1976). The mixture is liquid but appears crystalline under a polarizing microscope. It is therefore considered to be a form of liquid crystal (Brooks and Taylor, 1965; White, 1976). Mesophase in pyrobitumen is formed by a series of condensation reactions, generating polycyclic aromatic hydrocarbons as liquid crystal molecules (Lewis, 1980). Increasing temperature combines the liquid crystal molecules and discharges the low-boiling composition (White, 1976). Concentrated liquid crystal molecules then form layered mesophase lamellae (White, 1976; Lewis, 1980). Liquid crystal molecules in high graphitization level mesophase have a graphitic architecture, and dehydrogenation under extremely high temperatures would, in fact, turn it into graphite (White, 1976; Klett et al., 2000). However, the temperature required for complete dehydrogenation is over 1000 °C (Klett et al., 2000), which is not attainable in oil reservoirs.

Studies of mesophase indicate that, to form domain mesophase, the temperature must be high enough (over 300 °C) to keep the

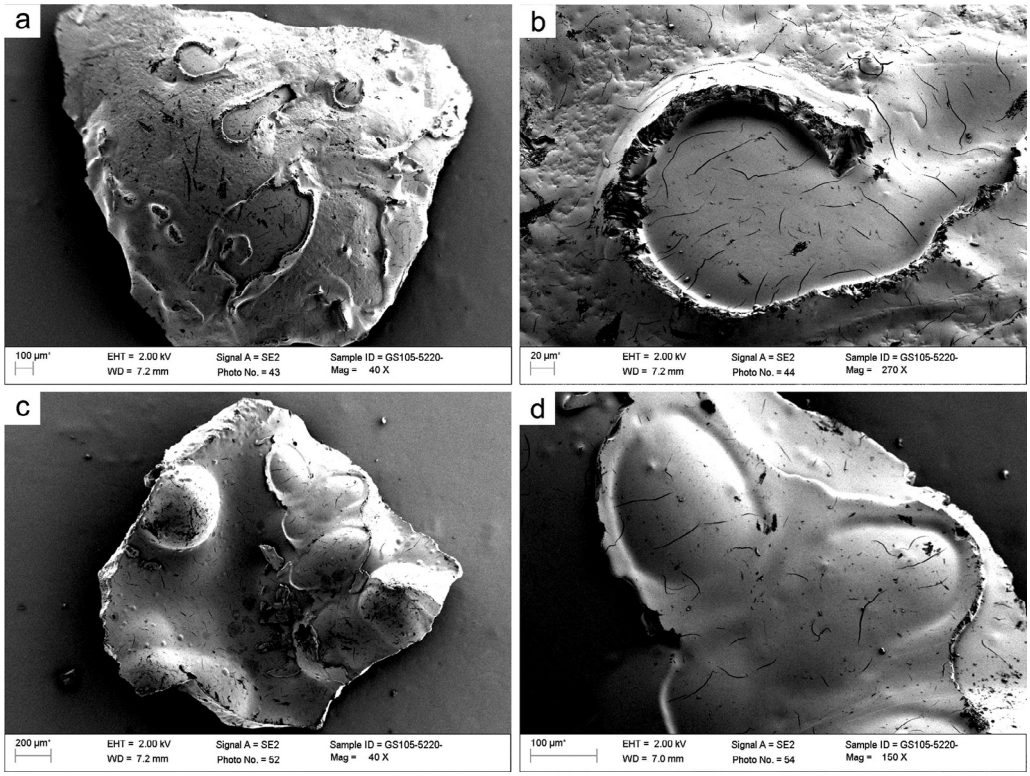

Fig. 6. SEM photomicrographs of a pyrobitumen piece peeled from the wall of a pore in the dolostone reservoir, Well GS105, 5220 m: (a) the convex surface of the pyrobitumen piece showing molds of escaped gas bubbles; (b) crateriform mold, formed by a bursting bubble; (c) the concave surface of the pyrobitumen piece showing moulage formed by bubbles in the pore; (d) moulage with a hemline.

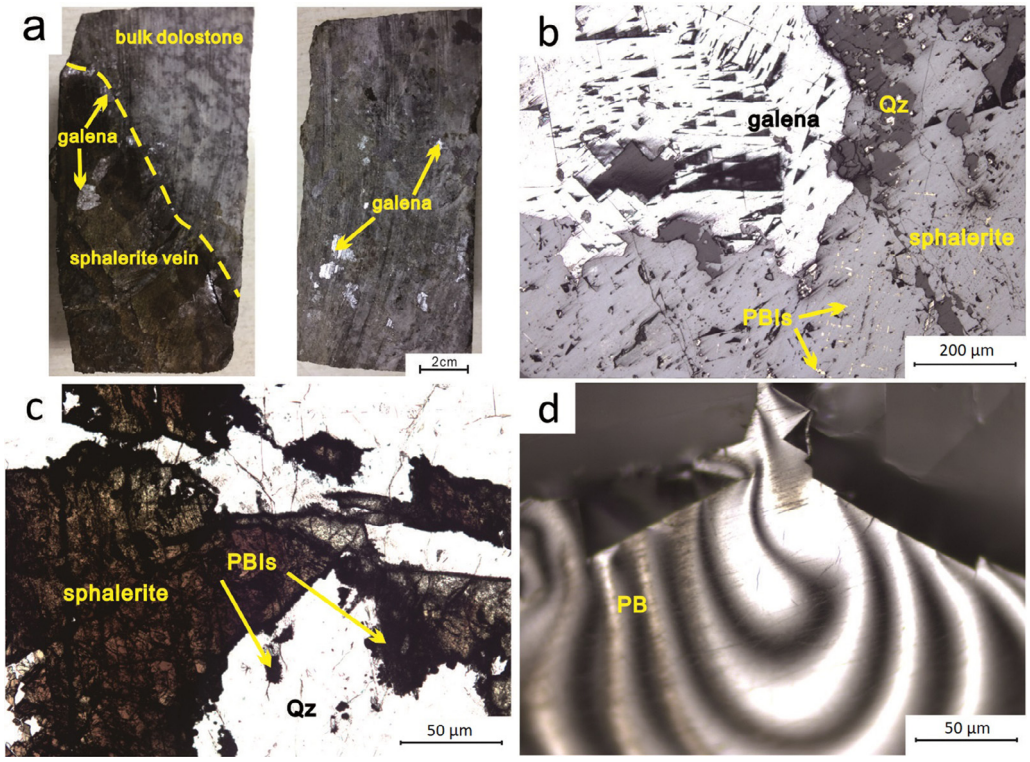

Fig. 7. Photomicrographs of MVT lead–zinc deposits and pyrobitumen in cores from the carbonate reservoir. Qz = quartz, PBIs = pyrobitumen inclusions, PB = pyrobitumen, P = plane-polarized transmission light, PRF = plane-polarized reflected light: (a) core samples from Well GS101, 5177 m; (b) a polished section of MVT lead–zinc under unpolarized reflected light, Well GS101, 5177 m, (PRF); (c) a thin polished section of MVT lead–zinc under plane-polarized transmitted light, Well GS101, 5177 m, (P); (d) polished section of pyrobitumen, Well GS105, 5220 m, (PRF).

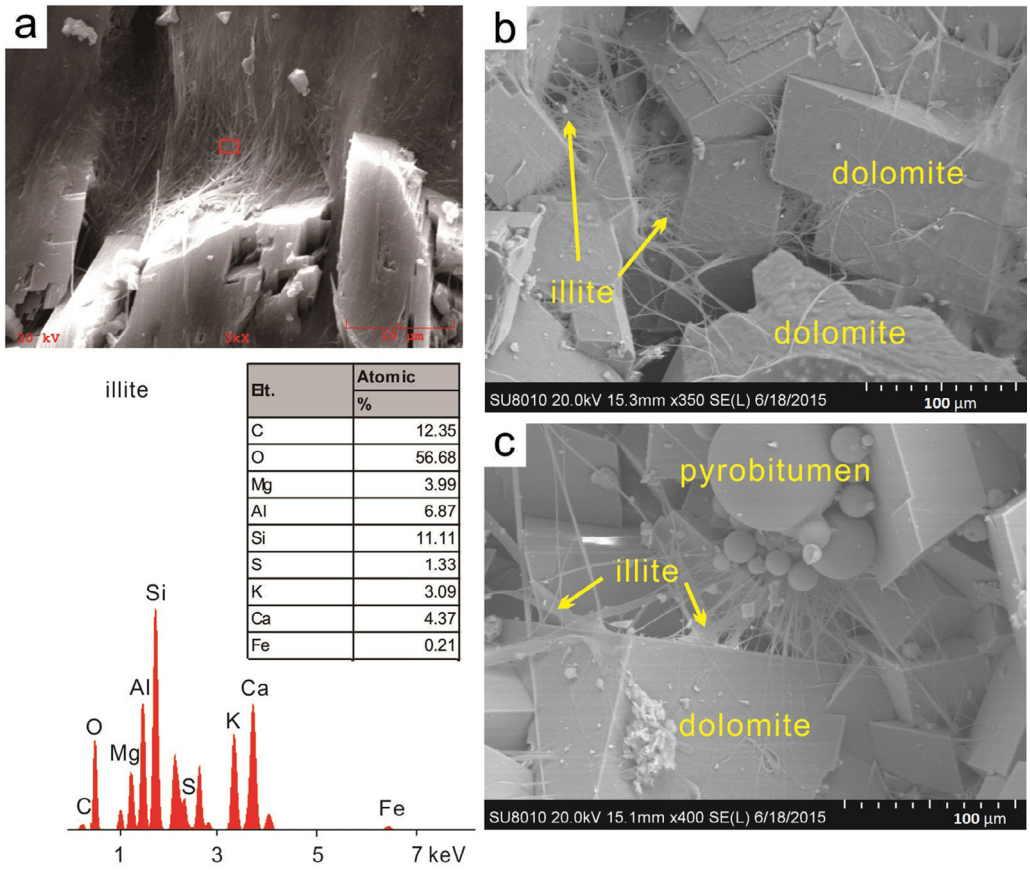

Elt.	Atomic %
C	12.35
O	56.68
Mg	3.99
Al	6.87
Si	11.11
S	1.33
K	3.09
Ca	4.37
Fe	0.21

Fig. 8. SEM-ESD characteristics of hydrothermal minerals in the Cambrian reservoir: (a) EDS characteristics of autogenetic illite, coated on saddle dolomite, Well MX204, 4652 m; (b) autogenetic illite in pores of the dolostone reservoir, Well MX205, 4599 m; (c) autogenetic illite in cracks of the dolostone reservoir accompanied by spherical pyrobitumens, Well MX204, 4656 m.

Table 2
Anisotropic texture and reflectance of pyrobitumen in the dolostone reservoir.

Well	Stratigraphy	Depth (m)	Lithology	%BRo_{max}	Optical texture
MX12	Cambrian	4659	dolostone	5.55	grain
mx204		4649		5.44	
mx204		4681		5.89	
mx56		4956		5.74	
GS17		4968	shale	3.66	isotropic matrix
GS1	Ediacaran	4977	dolostone	5.92	grain-domain
GS2		5013		6.95	
MX9		5033		6.24	
GS105		5220		7.74	flow-domain
GS7		5328		7.49	flow-domain
MX8		5425		7.34	domain

mesophase liquid, while the low-boiling composition must be discharged from the reservoir (White, 1976; Lewis, 1980; Tian 2013). The burial history of the Ediacaran reservoir shows that the maximum depth was over 8000 m, and the corresponding formation temperature was 220–230 °C. The stratigraphic burial and heat-flow histories of the study area have been reconstructed in previous studies (Jiang et al., 2014; Zou et al., 2014; Zhu et al., 2015, 2016; Liu et al., 2018; Yang et al., 2018a,b). These studies show that the temperature of the reservoir was never higher than 250 °C, much lower than the formation temperature of mesophase. Thus, the pyrolyzation of the reservoir and production of mesophase were probably results of rapid heating by hydrothermal fluid.

Some studies have suggested that elapse of time may decrease the threshold temperatures of organic evolution under certain geological conditions (Waples, 2000; Spigolon et al., 2015). In this case, formation of mesophase at a temperature of 220–230 °C is not impossible (Brooks and Taylor, 1965; White, 1976). However, the softening point of the mesophase is not influenced by time. Enhancement of the class of mesophase in the pyrobitumen would enlarge the size of PAHs, which are the elementary units of mesophase (Lewis and Kovac, 1978, 1980, 1987; Forrest and Marsh, 1983; Goodarzi, 1984; Mochida, et al., 1984). Under increasing temperatures, larger size PAHs decrease the mobility of the mesophase and change the softening point of the mesophase as well as the pyrobitumen (Brooks and Taylor, 1965; White, 1976). Thus, the temperature indicates the specific class of the mesophase which curdles at that temperature (Tian 2013). Further increase of the temperature would soften the mesophase, with consequent

enlargement of the PAHs, forming higher class mesophase (Gentzis, and Goodarzi, 1993; Rimmer et al., 2015; Yang et al., 2018a). The amount of time spent at high temperature is irrelevant to the generation of domain mesophase. The softening point of domain mesophase is over 300 °C because of its vast molecular weight (Brooks and Taylor, 1965; White, 1976; Jacob, 1989; Tian, 2013). Deep burial at temperatures of 220–230 °C is not enough by itself to keep mesophase liquid. The occurrence of large amounts of domain mesophase in the reservoir is therefore solid evidence of a high temperature event (Gentzis and Goodarzi, 1993; Rimmer et al., 2015; Yang et al., 2018a).

As mentioned, the pyrobitumen in the Ediacaran reservoir mostly transformed into domain mesophase (Fig. 5). As the oil transformed to mesophase, it passed through a liquid crystal stage (Brooks and Taylor, 1965; White, 1976). In addition, the molds and moulage on domain mesophase in pyrobitumen pieces (Fig. 6) provide clear evidence of rapid heating in the dolostone reservoir (Fig. 9). Two conditions must have been met to form the molds and moulage: an extremely high temperature, and rapid temperature fluctuations. To form the domain mesophase, the pyrobitumen must have been liquid. Any reduction in temperature would solidify the pyrobitumen and prevent the PAHs from enlarging their size. Therefore, the temperature was continually higher than 300 °C, the softening point of domain mesophase (White, 1976; Jacob, 1989; Tian, 2013). While the domain mesophase was forming, it maintained a sticky liquid form in the high temperature conditions. Gases were captured in the sticky liquid, with escaping gas leaving molds and moulage on the mesophase surface. Rapid temperature fluctuations must have occurred to preserve the molds and moulage, because long-term high temperature conditions would obliterate the impressions of gas bubbles on the soft surface of the mesophase (Fig. 9). Thus, after heating to above 300 °C, the temperature must have rapidly decreased, solidifying the pyrobitumen and preserving the molds and moulage on the domain mesophase. An abrupt hydrothermal fluid incursion is the only geological process that could have provided this rapid temperature fluctuation.

The abnormally low $\%BR_{omax}$ (3.66%) and isotropic microtexture of the pyrobitumen in the source rocks also indicate that hydrothermal fluid was the principal heat source for oil cracking and pyrobitumen generation in the dolostone reservoir (Yang et al., 2018a). Long-term burial would have slowly heated the strata, with the temperature of the formation controlled by a geothermal gradient determined by the heat flow and thermal conductivity of the rock (Zhu et al., 2016; Liu et al., 2018). The temperatures of specific formations therefore depend on their burial depths. Although the heat conductivities of the dolostone and the source rock are different, it is difficult to confirm any significant difference in the formation temperatures at the same depth (Zhu et al., 2016; Liu et al., 2018). The rapidity of hydrothermal fluid incursions depends on the permeability of the rocks. The shale was cooler, due to its lower permeability, so the pyrobitumen remained in the isotropic matrix grade. The data show that the pyrobitumen in the source rock was isotropic matrix with a lower $\%BR_{omax}$ (3.66%) which indicates a much lower temperature than that of the dolostone reservoir at the same depth (Table 2).

Observation of numerous cores in former studies has suggested that MVT lead–zinc deposits cover the entire paleo-oil reservoir (Jiang et al., 2016; Liu et al., 2016; Yang et al., 2018b; Zhang et al., 2019). MVT lead–zinc deposits occur widely around the world, including North America and Europe (Heyl et al., 1974; Anderson and Macqueen, 1982; Leach et al., 2005, 2010; Paradis et al., 2007) as well as South China (Li et al., 2007; Yin et al., 2009). Lead-zinc veins are a common indicator of high temperature conditions created by hydrothermal fluid invasions, with a fluid inclusion thermometry range of 50–250 °C (Basuki and Spooner, 2004). Hydrothermal fluid incursions can be triggered by the circulation of surface water in deep strata through faults or volcanic activity, which usually leads to higher temperatures (over 300 °C) in the fluids (Leach et al., 2005, 2010). It appears certain that the high temperature conditions required to form high class mesophase in the reservoir were triggered by the ELIP, which provided the driving force and thermal energy for the invading hydrothermal fluids. The migration route of the hydrothermal

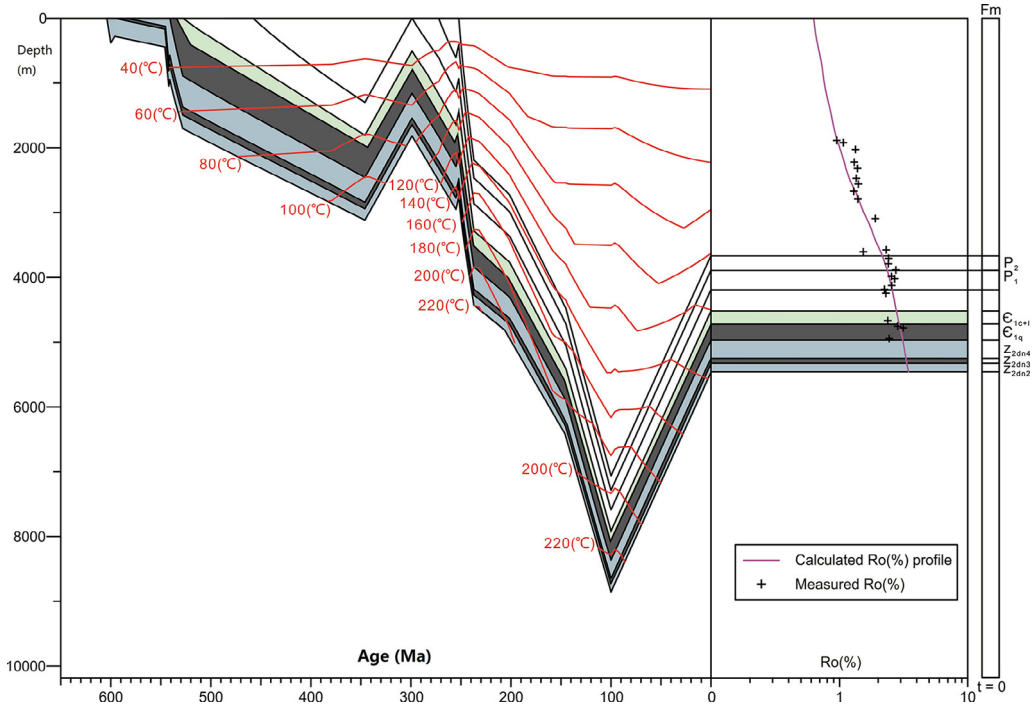

Fig. 9. Reconstructed stratigraphic burial, thermal history, and paleo-heat flow history plots for Well GS6, R_o modeled-maturity profiles and diagenesis sequence (Yang et al., 2018a).

fluid, according to the distribution of hydrothermal minerals (Figs. 7, 8) and pyrobitumen (Table 2), was from the southwest to the northeast of the Chuanzhong Uplift, and from the Ediacaran reservoir (or deeper strata) to the Cambrian reservoir. The path of the hydrothermal fluid followed the relatively high permeability layers of the successions (Yang et al., 2018a).

5.2. Dating of the thermal event

Time and temperature are the key factors in oil cracking. However, pinpointing the timing of occurrence of pyrolysis is difficult because of the complicated chemical conditions during long term diagenetic processes in reservoirs (Yang et al., 2018a,b) and the lack of suitable dating minerals. The reservoir in the Yangtze Block has been buried for a long time over 600 Myr, thus diagenetic processes have overprinted information in the minerals that could be used to date early events in geological time. Moreover, because of the great burial depth of the reservoir, sampling relies on well cores, so appropriate dating minerals are difficult to obtain. An alternative is to apply cross-validation to the various pieces of evidence that are available. The discovery of mesophase and the testing of inclusions confirm that the reservoir's long-term burial could not have provided a sufficiently high temperature for the formation of domain mesophase (Yang et al., 2018a,b). However, the present study reveals that all the Ediacaran reservoirs in the Chuanzhong Uplift were filled with hydrothermal fluid and domain mesophase (Jiang et al., 2014; Zou et al., 2014; Zhu et al., 2015; Yang et al., 2018a,b). The ELIP was the only significant thermal event in the area that could have produced hydrothermal fluid on such a vast scale. Magma eruptions during the event may have pushed against adjacent strata and triggered a hydrothermal fluid invasion into the reservoir. Pyrolysis of the liquid oil would have rapidly converted the oil into gas and pyrobitumen (Yang et al., 2018a). The timing of the hydrothermal fluid invasion, and thus of liquid oil pyrolysis, can be obtained by reconstruction of the stratigraphic burial and geothermal histories.

The geothermal history has previously been reconstructed from apatite fission tracks (Zhu et al., 2016; Liu et al., 2018) (Fig. 10). Consistency between the simulated and measured reflectance of vitrinite-like macerals in source rocks confirms the reliability of the geothermal history established in a previous report by the present authors (Zhu et al., 2016; Liu et al., 2018; Yang et al., 2018a,b). The hydrothermal fluid invasion can be correlated to the ELIP during the Late Permian, when heat flow abruptly rose (Liu et al., 2018) (Fig. 10). The reconstructed heat flow history confirms that there was only one major thermal event during the entire burial history of the reservoir (Fig. 10). Therefore, the huge invasion of hydrothermal fluid must have been triggered by the basin-scale thermal event that can be clearly observed on the heat flow history curves (Fig. 10). The ELIP, in the late Permian, is the most likely candidate for this event. Magma did not directly affect the reservoir, despite the proximity of the ELIP (Fig. 1a). The rapid rise in heat flow in the Chuanzhong Uplift was therefore probably due to heating of the hydrothermal fluid by magma in deep strata. Once the hydrothermal fluid was hot, it started to upwell, bringing minerals and heat to the sedimentary cover of the basin (Davies and Smith, 2006; Paradis et al., 2007; Jiang et al., 2016). The pathway of the hydrothermal fluid was along faults in the Chuanzhong Uplift, including the NE trending strike-slip fault and the normal fault, which might have connected with the basement along the western edge of the Anyue gas field (Wei et al., 2013; Zou et al., 2014; Zhu et al., 2015; Yang et al., 2018a,b). On this basis, hydrothermal fluid invasion is the most reasonable interpretation for the increased heat flow during the late Permian (Fig. 10).

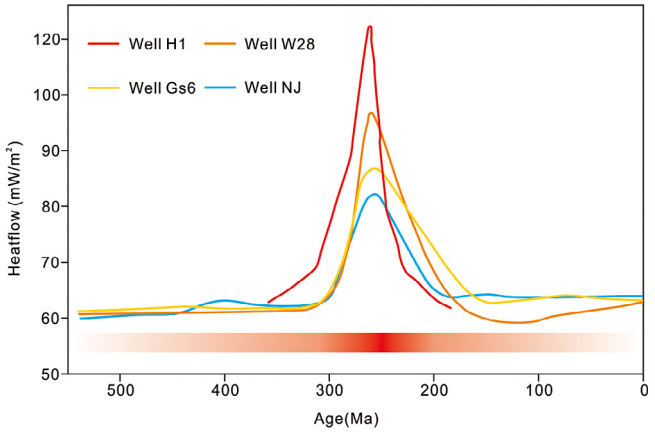

Fig. 10. Reconstructed paleo-heat flow history plots for wells in the center of the Sichuan Basin (modified after Zhu et al., 2016; Liu et al., 2018).

One of the most recent studies, by Zhong et al. (2014), reported the age of the ELIP as 259.1 ± 0.5 Ma. The main activity period of a large igneous province is usually around 50Myr, with 75% of the magma rising to the surface within 1–5 Myr (Bryan and Ernst, 2008, 2013). The period of abnormal thermal conditions and the hydrothermal fluid invasion related to the ELIP might therefore have occurred at approximately 260 ± 5 Ma. Consequently, the timing of oil pyrolysis could be related to both the GLE (~260 Ma) and PTE (~252 Ma), since the precise timing of oil pyrolysis might not align perfectly with the occurrence of the ELIP. However, currently available data indicate that oil pyrolysis was closely linked to the GLE during the LPC.

5.3. Gas release from the reservoirs

Massive amounts of volatile components were generated in the Ediacaran reservoir during the pyrolysis process. Simulation experiments indicate that these volatile substances were mostly methane and carbon dioxide (Spigolon et al., 2015). The gases must have been rapidly released from the reservoir, and the concentrated liquid crystal molecules would then have formed layered mesophase lamellae (White, 1976; Lewis, 1980). During the hydrothermal fluid incursion, pipes might have formed as a consequence of pressure build-up, allowing gases to vent from the reservoir to the surface (Ganino and Arndt, 2009; Svensen et al., 2009; Jerram et al., 2015). In the similar case of the Tunguska Basin in Russia, ejection of magma, triggered by the Siberian Traps, led to gas generation in organic-rich shales, followed by evaporation and petroleum accumulation (Svensen et al., 2009). Gas-induced venting occurred through pipes reaching from depths of over 2000 m to the surface (Svensen et al., 2009). However, the temperature of the hydrothermal fluid in the Chuanzhong Uplift was much lower than that of the Tunguska magma. The temperature of magma is over 1000 °C, while the mesophase indicates that the temperature of the hydrothermal fluid in the reservoir in the Chuanzhong Uplift was approximately 300 °C. At this temperature, metamorphic devolatilization of carbonates and consequent generation of gases may not have occurred. However, the temperature of the hydrothermal fluid was sufficient to pyrolyze the oil (Yang et al., 2018b) with the hydrothermal fluid entering pores more easily than magma and therefore heating the oil more thoroughly (Yang et al., 2018a).

At the time of the hydrothermal fluid invasion caused by the ELIP, the sealing cap rocks in the Ediacaran reservoirs were generally less than 1500 m thick (Du et al., 2014), indicating that overburden pressure of the pyrolysis gases was much lower than in the Tunguska Basin (Svensen et al., 2009). The Ediacaran reservoir is now covered by thick successions of overlying formations. How-

ever, seismic data reveal faults and potential pipes contemporaneous with the ELIP in the Chuanzhong Uplift (Fig. 11) (Yang et al., 2017). The pyrolysis of oil could have contributed significantly to pipe formation, as cracking under atmospheric conditions results in a 700-fold increase in volume (Barker, 1990). The pipes could have penetrated the sealing cap rocks and released gases into the water column and atmosphere within a relatively short span of time (Fig. 12). The seismic data are not the only evidence of pipes in the sealing cap rocks. Other studies have revealed masses of breccia (Fig. 2b, c, d), caves, and cracks, accompanied by hydrothermal fluid, in the Ediacaran reservoir in the Chuanzhong Uplift (Wei et al., 2013; Zou et al., 2014; Zhu et al., 2015; Jiang et al., 2016) which may be the remains of pipe structures. However, these could also have been formed by karstification (Loucks et al., 2004). Because the reservoirs are now deeply buried, the limited well samples available are not able to distinguish between karstification and gas venting. However, the mesophase, the hydrothermal fluid, and the seismic data, as well as the analogy of the Tunguska Basin event (Svensen et al., 2009), can be taken together to support the implication that gas venting occurred in the Chuanzhong Uplift.

The ELIP may have triggered a major thermal event in the late Permian, causing hydrothermal fluid to invade the Ediacaran reservoir (Fig. 12). The oil in the reservoir would have been rapidly heated, forming pyrobitumen and volatile components including methane (CH_4) and carbon dioxide (CO_2). Hydrogen sulfide (H_2S) might also have been produced by thermochemical sulfate reduction (TSR) (Zhu et al., 2015; Liu et al., 2016). These gases were then rapidly released through pipes (Fig. 12), while the pyrobitumen with high class mesophase remained in the reservoir (Figs. 5, 6).

5.4. Relevance to the LPC

Considerable research has strongly suggested that global warming is likely to have been one of the mechanisms for the LPC—the most severe biotic crisis so far in Earth's history (Shu et al., 2011; Joachimski et al., 2012). The vast volumes of greenhouse gases, primarily CH_4 and CO_2, among pyrolytic gases generated in paleo-oil reservoirs could have contributed significantly to the global warming effect (Ganino and Arndt, 2009; Svensen et al., 2009). Estimated geological oil reserves in the Ediacaran Paleo-oil reservoir are approximately 6×10^9 tons (Zou et al., 2014). Previous simulation experiments have shown that the gas (C_1–C_4) transformation rate during oil pyrolysis is up to 400 mg/g oil (Schenk et al., 1997). Therefore, the oil in the paleo-oil reservoir could, in principle, have been converted into approximately 2.4×10^{15} g of natural gas. Consequently, it can be speculated that up to $1.9\ (2.4–0.5) \times 10^{15}$ g natural gas was released into the water column and atmosphere. Previous studies have shown that approximately 1.1×10^{18} g of methane expelled from hydrate ($\delta^{13}C = -60‰$) is sufficient to cause an approximately 2.5‰ negative excursion in carbon isotopes and a more than 6 °C increase in temperature during the IETM (Erwin, 1994; Xie et al., 2007). In this case, the gases released from the Ediacaran reservoir in the Chuanzhong Uplift would not have been enough to drive such a large negative excursion and temperature increase. However, the Ediacaran reservoir in the Chuanzhong Uplift is only one of many paleo-oil reservoirs in the YB. A series of paleo-oil reservoirs, with over one billion tons of oil accumulated during the Late Carboniferous–Early Permian, has been discovered near the ELIP along the south edge of the YB (Bo et al., 2012). Discovery of mesophase in pyrobitumen indicates that several of these reservoirs might also have been strongly impacted by a tectonic-thermal event during the LPC (Shi et al., 2015). If this episode of volcanism occurred on a global scale, it could easily have pyrolyzed a significant proportion of the oils accumulated in pre-Permian marine successions. The enormous volumes of methane expelled by pyrolysis of these oils might have contributed significantly to driving radical climate change during the LPC.

In addition to large volumes of CH_4 and CO_2 from gas hydrates, the leaks of gas from the reservoir probably also contained H_2S, which is lethal to most fauna on Earth (Knoll and Grotzinger, 1996). In reservoirs, contact metamorphism of organic materials under burial conditions produces H_2S in thermochemical sulfate reduction (TSR) reactions (Cai et al., 2003; Liu et al., 2016; Zhang et al., 2019). Gypsum in the Ediacaran strata could have supplied sulfate, and the hydrothermal fluid could have provided sufficient heat for TSR to occur (Liu et al., 2016; Zhang et al., 2019). However, the normal burial process might also have provided sufficient heat

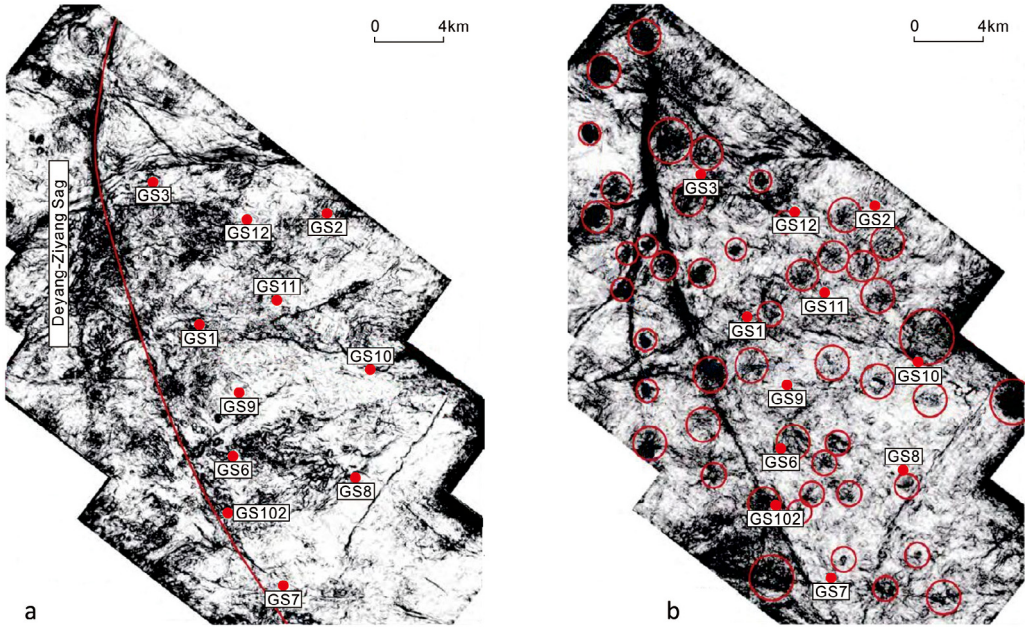

Fig. 11. Seismic slices of coherent attributes on the bottom of the Ediacaran reservoir: (a) 120 ms (ca. 200 m) above the top of the Ediacaran reservoir; (b) modified after Yang et al. (2017).

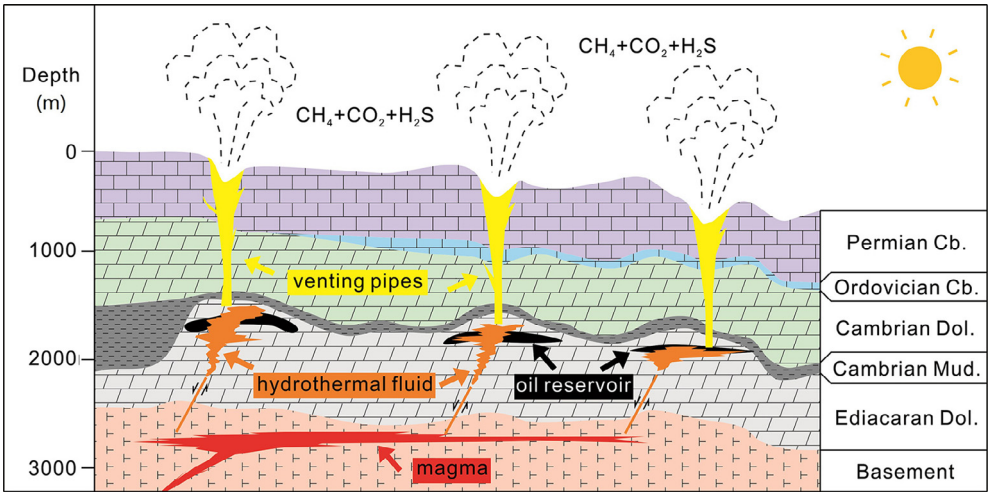

Fig. 12. Schematic model of oil pyrolysis and venting of carbon gases and halocarbons to the atmosphere through pipes in the Chuanzhong Uplift. The pipes are partly modeled on those found in the Tunguska Basin (after Svensen et al., 2009).

for TSR long after the thermal event of the late Permian. It is therefore difficult to confirm whether all the hydrogen sulfide produced by TSR was related to the thermal event in the Chuanzhong Uplift.

6. Conclusion

Systematic analysis of core samples from the Ediacaran reservoir in the Chuanzhong Uplift suggests that the paleo-oil reservoir was pyrolyzed by hydrothermal fluid. The hydrothermal fluid was associated with a basin-scale thermal event, probably triggered by the ELIP in the late Permian. The presence of high maturity pyrobitumen indicates that oil was rapidly pyrolyzed and the gases generated were discharged from the reservoir. A set of pipes has been discovered leading from the upper strata of the Ediacaran reservoir to the surface, suggesting that the gases generated by rapid pyrolysis of oil in the reservoir might have been instantaneously released into the atmosphere. It can therefore reasonably be concluded that paleo-oil reservoir pyrolysis could have released massive quantities of natural gas from Paleozoic reservoir rocks all around the Yangtze Block within a relatively short span of time. However, dating such an ancient hydrothermal event either by minerals or organic matter is difficult through the conventional methods. Therefore, in this study, multiple pieces of evidence were cross validated to provide a timing for the oil pyrolysis and gas release in the Ediacaran reservoir. Hydrothermal mineralization, high graphitized mesophase in pyrobitumen, and analysis of methane inclusions in the reservoir all point to a thermal event driven by hydrothermal fluid invasion. In addition, the seismic data provide evidence of gas venting through pipes in the upper strata of the Ediacaran reservoir. Therefore, although there are still points of inconsistency, the model of hydrothermal oil pyrolysis and sudden gas release is a reasonable inference.

Cases of paleo-oil reservoirs cracking as a result of volcanic activity are difficult to identify because the reservoirs are now deep below the surface. However, the estimate of the gas volume released in the event in the Chuanzhong Uplift suggests that it could have been on a sufficient scale to be the mechanism, or at least one of the mechanisms, for the Late Permian Crisis. There are huge numbers of other basins around the world that have paleo-oil reservoirs in pre-Permian strata. Volcanic activity might also have pyrolyzed the oil in other paleo-oil reservoirs, rapidly releasing enormous volumes of greenhouse and other toxic gases into the atmosphere and thereby also contributing to the Late Permian Crisis.

Declaration of Competing Interest

The authors declare that they have no known competing financial interests or personal relationships that could have appeared to influence the work reported in this paper.

Acknowledgements

This work was funded by the National Natural Science Foundation for Young Scholars of China (Grant No. 41903059) and the National Key Technologies Research and Development Program of China (Grant No. 2017YFC0603102). The authors are grateful to Dr. Steve Larter from the University of Calgary for his constructive suggestions and revision of the original manuscript.

References

Anderson, G.M., Macqueen, R.W., 1982. Ore deposit models-6. Mississippi Valley-type lead–zinc deposits. Geosci. Can. 9, 107–117.
Barker, C., 1990. Calculated volume and pressure changes during the cracking of oil and gas in reservoirs. AAPG Bull. 74, 1254–1261.
Basuki, N.I., Spooner, E.T.C.A., 2004. Review of fluid inclusion temperatures and salinities n Mississippi Valley-type Zn-Pb deposits: identifying thresholds for metal transport. Explor. Min. Geol. 11, 1–17.
Becker, L., Poreda, R.J., Hunt, A.G., Bunch, T.E., Rampino, M., 2001. Impact event at the Permian-Triassic boundary: evidence from extraterrestrial noble gases in fullerenes. Science 291, 1530–1533.
Black, B.A., Elkins-Tanton, L.T., Rowe, M.C., Peate, I.U., 2012. Magnitude and consequences of volatile release from the Siberian Traps. Earth Planet. Sci. Lett. 317-318, 363–373.
Braithwaite, C.J.R., Rizzi, G., 1997. The geometry and petrogenesis of hydrothermal dolomites at Navan, Ireland. Sedimentology 44 (3), 421–440.
Brooks, J.D., Taylor, G.H., 1965. Formation of Graphitizing Carbons from the Liquid Phase. Nature 206 (4985), 697–699.
Bryan, S.E., Ernst, R.E., 2008. Revised definition of Large Igneous Provinces (LIPs). Earth-Sci. Rev. 86 (1-4), 175–202.
Bryan, S.E., Ferrari, L., 2013. Large igneous provinces and silicic large igneous provinces: Progress in our enderstanding over the last 25 years. GSA Bull. 125 (7–8), 1053–10178.
Burgess, S.D., Muirhead, J.D., Bowring, S.A., 2017. Initial pulse of Siberian Traps sills as the trigger of the end-Permian mass extinction. Nat. Commun. 8, 164.
Cai, C., Worden, R.H., Bottrell, S.H., Wang, L., Yang, C., 2003. Thermochemical sulphate reduction and the generation of hydrogen sulphide and thiols (mercaptans) in Triassic carbonate reservoirs from the Sichuan Basin. China. Chem. Geol. 202, 39–57.

Chuhan, F.A., Bjørlykke, K., Lowrey, C., 2000. The role of provenance in illitization of deeply buried reservoir sand- stones from Haltenbanken and North Viking Graben, Offshore Norway. Mar. Pet. Geol. 17, 673–689.
Chung, S.L., Jahn, B.M., 1995. Plume-lithosphere interaction in generation of the Emeishan flood basalts at the Permian-Triassic boundary. Geology 23, 889.
Clapham, M.E., Payne, J.L., 2011. Acidification, anoxia, and extinction: A multiple logistic regression analysis of extinction selectivity during the Middle and Late Permian. Geology 39, 1059-1062.
Clarkson, M.O., Kasemann, S.A., Wood, R.A., Lenton, T.M., Daines, S.J., Richoz, S., Ohnemueller, F., Meixner, A., Poulton, S.W., Tipper, E.T., 2015. Ocean acidification and the Permo-Triassic mass extinction. Science 348, 229–232.
Cui, Y., Kump, L.R., 2014. Global warming and the end-Permian extinction event: Proxy and modeling perspectives. Earth-Sci. Rev. 149, 5–22.
Davies, G.R., Smith, L.B., 2006. Structurally controlled hydrothermal dolomite reservoir facies: An overview. AAPG Bull. 90 (11), 1641–1690.
Ding, J., Zhang, L., Zhang, Y., Han, K.L., 2013. A reactive molecular dynamics study of n-heptane pyrolysis at high temperature. J. Phys. Chem. A. 117 (16), 3266–3278.
Du, J., Zou, C., Xu, C., He, H., Shen, P., Yang, Y., Li, Y., Wei, G., Wang, Z., Yang, Y., 2014. Theoretical and technical innovations in strategic discovery of a giant gas field in Cambrian Longwangmiao Formation of central Sichuan paleo-uplift, Sichuan Basin. Pet. Explor. Dev. 41, 294–305 (in Chinese with English abstract).
Elkins-Tanton, L.T., Grasby, S.E., Black, B.A., Veselovskiy, R.V., Ardakani, O.H., Goodarzi, F., 2020. Field evidence for coal combustion links the 252 Ma Siberian Traps with global carbon disruption. Geology 48 (10), 1–6.
Elrick, M., Polyak, V., Algeo, T.J., Romaniello, S., Asmerom, Y., Herrmann, A.D., Anbar, A.D., Zhao, L., Chen, Z.-Q., 2017. Global-ocean redox variation during the middle-late Permian through Early Triassic based on uranium isotope and Th/U trends of marine carbonates. Geology 45, 163–166.
Erwin, D.H., 1994. The Permo-Triassic extinction. Nature 367, 231–236.
Fairchild, I.J., 1983. Chemical controls of cathodoluminescence of natural dolomites and calcites: new data and review. Sedimentology 30, 579–583.
Feng, M., Wu, P., Qiang, Z., Liu, X., Duan, Y., Xia, M., 2017. Hydrothermal dolomite reservoir in the Precambrian Dengying Formation of central Sichuan Basin Southwestern China. Mar. Pet. Geol. 82, 206–219.
Forrest, M.A., Marsh, H., 1983. The effects of pressure on the carbonization of pitch and pitch/carbon fibre composites. J. Mater. Sci. 18 (4), 978–990.
Ganino, C., Arndt, N.T., 2009. Climate changes cause by degassing of sediments during the emplacement of large igneous provinces. Geology. 37 (4), 323–326.
Gao, P., Liu, G., Lash, G.G., Li, B., Yan, D., Chen, C., 2018. Occurrences and origin of reservoir solid bitumen in Sinian Dengying Formation dolomites of the Sichuan Basin, SW China. Int. J. Coal Geol. 200, 135–152.
Geng, A., Liao, Z., 2002. Kinetic studies of asphaltene pyrolyses and their geochemical applications. Appl. Geochem. 17 (12), 1529–1541.
Gentzis, T., Goodarzi, F., 1993. Maturity studies and source-rock potential in the southern Sverdrup Basin. Arctic Canada. Int. J. Coal Geol. 24 (1-4), 141–177.
Goodarzi, F., 1984. Organic petrology of graptolite fragments from Turkey. Mar. Pet. Geol. 1, 202–210.
Goodarzi, F., Norford, B.S., 1985. Graptolites as indicators of the temperature histories of rocks. J. Geol. Soc. 142 (6), 1089–1099.
Grasby, S.E., Sanei, H., Beauchamp, B., 2011. Catastrophic dispersion of coal fly ash into oceans during the latest Permian extinction. Nat. Geosci. 4, 104–107.
Grasby, S.E., Knies, J., Beauchamp, B., Bond, D.P.G., Wignall, P., Sun, Y.D., 2020. Global warming leads to Early Triassic nutrient stress across northern Pangea. GSA Bull. 132, 943-954.
Gregg, J.M., Karakus, M., 1991. A technique for successive cathodoluminescence and reflected light petrography. J. Sediment. Res. 61, 613–614.
He, B., Xu, Y.G., Chung, S.L., Xiao, L., Wang, Y., 2003. Sedimentary evidence for a rapid, kilometer-scale crustal doming prior to the eruption of the Emeishan flood basalts. Earth Planet. Sci. Lett. 213, 391–405.
Heyl, A.V., Landis, G.P., Zartman, R.E., 1974. Isotopic evidence for the origin of Mississippi Valley-type mineral deposits. Econ. Geol. 69, 992–1006.
Horsfield, B., Schenk, H.J., Mills, N., Welte, D.H., 1992. An investigation of the in-reservoir conversion of oil to gas: compositional and kinetic findings from closed-system programmed-temperature pyrolysis. Org. Geochem. 19, 191–204.
Hu, Y., Cai, C., Pederson, C.L., Liu, D., Jiang, L., He, X., Shi, S., Immenhauser, A., 2020. Dolomitization history and porosity evolution of a giant, deeply buried Ediacaran gas field (Sichuan Basin, China). Precambrian Res. 338, 105595.
Hudspith, V.A., Rimmer, S.M., Belcher, C.M., 2014. Latest Permian chars may derive from wildfires, not coal combustion. Geology 42, 879–882.
Jacob, H., 1989. Classification, structure, genesis and practical importance of natural solid oil bitumen ("migrabitumen"). Int. J. Coal Geol. 11, 65–79.
Jerram, D.A., Widdowson, M., Wignall, P.B., Sun, Y.D., Lai, X.L., Bond, D.P.G., Torsvik, T.H., 2015. Submarine palaeoenvironments during Emeishan flood basalt volcanism, SW China: Implications for plume–lithosphere interaction during the Capitanian, Middle Permian ('end Guadalupian') extinction event. Palaeogeogr. Palaeoclimatol. Palaeoecol. 441, 65–73.
Jiang, H., Wang, Z.C., Du, H.Y., Zhang, C.M., Wang, R.J., Zou, N.N., Wang, T.S., Gu, Z.D., Li, Y.X., 2014. Tectonic evolution of the Leshan-Longnvsi Paleo-uplift and reservoir formation of Neoproterozoic Sinian Gas. Nat. Gas Geosci. 25, 192–200 (in Chinese with English abstract).
Jiang, Y., Tao, Y., Gu, Y., Wang, J., Qiang, Z., Jiang, N., Lin, G., Jiang, C., 2016. Hydrothermal dolomitization in Dengying Formation, Gaoshiti-Moxi area, Sichuan Basin, SW China. Pet. Explor. Dev. 43, 54–64 (in Chinese with English abstract).
Jin, Y.G., Mei, S.L., Wang, W., Wang, X.D., Shen, S.Z., Shang, Q.H., Chen, Z.Q., 1998. On the Lopingian Series of the Permian System. Palaeoworld 9, 1–18.
Joachimski, M.M., Lai, X., Shen, S., Jiang, H., Luo, G., Chen, B., Chen, J., Sun, Y., 2012. Climate warming in the latest Permian and the Permian-Triassic mass extinction. Geology 40, 195–198.
Klett, J., Hardy, R., Romine, E., Walls, C., Burchell, T., 2000. High-thermal-conductivity, mesophase-pitch-derived carbon foams: effect of precursor on structure and properties. Carbon 38, 953–973.
Kirschvink, J.L., Isozaki, Y., Shibuya, H., Otofuji, Y.-I., Raub, T.D., Hilburn, I.A., Kasuya, T., Yokoyama, M., Bonifacie, M., 2015. Challenging the sensitivity limits of Paleomagnetism: Magnetostratigraphy of weakly magnetized Guadalupian-Lopingian (Permian) Limestone from Kyushu, Japan. Palaeogeogr., Palaeoclimatol. Palaeoecol. 418, 75–89.
Knoll, A.H., Bambach, R.K., Payne, J.L., Pruss, S., Fischer, W.W., 2007. Paleophysiology and end-Permian mass extinction. Earth Planet. Sci. Lett. 256 (3-4), 295–313.
Knoll, A.H., Bambach, R.K., Canfield, D.E., Grotzinger, J.P., 1996. Comparative earth history and Late Permian mass extinction. Science 273 (5274), 452–457.
Leach, D.L., Sangster, D.F., Kelley, K.D., Large, R.R., Garven, G., Allen, C.R., Gutzmer, J., Walters, S.G., 2005. Sediment-hosted lead-zinc deposits-a global perspective. Soc. Econ. Geol. 100, 561–607.
Leach, D.L., Bradley, D.C., Huston, D., Pisarevsky, S.A., Taylor, R.D., Gardoll, S.J., 2010. Sediment-hosted Lead-Zinc-Deposits in earth history. Econ. Geol. 105 (3), 593–625.
Lewis, I.C., Kovac, C.A., 1978. The role of free radicals and molecular size in mesophase pitch. Carbon 16 (6), 425–429.
Lewis, I.C., 1980. Thermal polymerization of aromatic hydrocarbons. Carbon 18, 191–196.
Lewis, I., 1987. Chemistry of pitch carbonization. Fuel 66 (11), 1527–1531.
Li, W., Huang, Z., Yin, M., 2007. Dating of the Giant Huize Zn-Pb Ore field of Yunnan Province, Southwest China: constraints from the Sm-Nd system in hydrothermal calcite. Resour. Geol. 57 (1), 90–97.
Liu, Q., Zhu, D., Jin, Z., Liu, C., Zhang, D., He, Z., 2016. Coupled alteration of hydrothermal fluids and thermal sulfate reduction (TSR) in ancient dolomite reservoirs – An example from Sinian Dengying Formation in Sichuan Basin, southern China. Precambrian Res. 285, 39–57.
Liu, W., Qiu, N., Xu, Q., Liu, Y., 2018. Precambrian temperature and pressure system of Gaoshiti-Moxi block in the central paleo-uplift of Sichuan Basin, southwest China. Precambrian Res. 313, 91–108.
Lorant, F., Behar, F., Vandenbroucke, M., Mckinney, D.E., Tang, Y.C., 2000. Methane generation from methylated aromatics: kinetic study and carbon isotope modeling. Energy Fuel 14 (6), 1143–1155.
Loucks, R.G., Mescher, P.K., Mcmechan, G.A., 2004. Three-dimensional architecture of a coalesced, collapsed-paleocave system in the Lower Ordovician Ellenburger Group, central Texas. AAPG Bull. 88 (5), 545–564.
Loyd, S.J., Corsetti, F.A., Eagle, R.A., Hagadorn, J.W., Shen, Y., Zhang, X., Bonifacie, M., Tripati, A.K., 2015. Evolution of Neoproterozoic Wonoka-Shuram Anomaly-aged carbonates: Evidence from clumped isotope paleothermometry. Precambrian Res. 264, 179–191.
Machel, H.G., 1985. Cathodoluminescence in calcite and dolomite and its chemical interpretation. Geosci. Canada 12, 139–147.
Mastalerz, M., Agnieszka, D., Stankiewicz, A.B., 2018. Origin, properties, and implications of solid bitumen in source-rock reservoirs: A review. Int. J. Coal Geol. 195, 14–36.
Milner, C.W.D., Rogers, M.A., Evans, C.R., 1977. Petroleum transformations in reservoirs. J. Geochem. Explor. 7, 101–153.
Mochida, I., Korai, Y., Fujitsu, H., Takeshita, K., Komatsubara, Y., Koba, K.I., Marsh, H., 1984. Aspects of gasification and structure in cokes from coals. Fuel. 63, 136–139.
Paradis, S., Hannigan, P., Dewing, K., 2007. Mississippi Valley-type lead-zinc deposits (MVT). Mineral Deposits of Canada 5.
Penn, J.L., Deutsch, C., Payne, J.L., Sperling, E.A., 2018. Temperature-dependent hypoxia explains biogeography and severity of end-Permian marine mass extinction. Science 362, eaat1327.
Pierson, B.J., 1981. The control of cathodoluminescence in dolomite by iron and manganese. Sedimentology 28, 601–610.
Pluijm, B., Hall, C.M., Vrolijk, P.J., Pevear, D.R., Covey, M., 2001. The dating of shallow faults in the Earth's crust. Nature 412 (6843), 172–175.
Ragan, S., Marsh, H., 1981. Carbonization and liquid-crystal (mesophase) development. 22. Micro-strength and optical textures of cokes from coal-pitch co-carbonizations. Fuel 60, 522–528.
Rahl, J.M., Haines, S.H., Pluijm, B., 2011. Links between orogenic wedge deformation and erosional exhumation: evidence from illite age analysis of fault rock and detrital thermochronology of syn-tectonic conglomerates in the Spanish pyrenees. Earth Planet. Sci. Lett. 307 (1–2), 180–190.
Rimmer, S.M., Crelling, J.C., Yoksoulian, L.E., 2015. An occurrence of coked bitumen, Raton Formation, Purgatoire River Valley, Colorado, U.S.A. Int. J. Coal Geol. 141–142, 63–73.
Rippen, D., Littke, R., Bruns, B., Mahlstedt, N., 2013. Organic geochemistry and petrography of Lower Cretaceous Wealden black shales of the Lower Saxony Basin: the transition from lacustrine oil shales to gas shales. Org. Geochem. 63, 18–36.
Roscher, M., Stordal, F., Svensen, H., 2011. The effect of global warming and global cooling on the distribution of the latest Permian climate zones. Palaeogeogr., Palaeoclimatol., Palaeoecol. 309.
Sanei, H., 2020. Genesis of solid bitumen. Sci. Rep. 10, 15595.

Schenk, H.J., Di, P.R., Horsfield, B., 1997. The conversion of oil into gas in petroleum reservoirs. Part 1: Comparative kinetic investigation of gas generation from crude oils of lacustrine, marine and fluviodeltaic origin by programmed-temperature closed-system pyrolysis. Org. Geochem. 26, 467–481.

Shi, C.H., Cao, J., Bao, J.P., Zhu, C.S., Jiang, X.C., Wu, M., 2015. Source characterization of highly mature pyrobitumens using trace and rare earth element geochemistry: Sinian-Paleozoic paleo-oil reservoirs in South China. Org. Geochem. 83–84, 77–93.

Shu, Z.S., Crowley, J.L., Wang, Y., Bowring, S.A., Erwin, D.H., Sadler, P.M., Cao, C.Q., Rothman, D.H., Henderson, C.M., Ramezani, J., Zhang, H., Shen, Y.N., Wang, X.D., Wang, W., Mu, L., Li, W.Z., Tang, Y.G., Liu, X.L., Liu, L.J., Zeng, Y., Jiang, Y.F., Jin, Y. G., 2011. Calibrating the end-Permian mass extinction. Science 334, 1367–1372.

Spigolon, A.L.D., Lewan, M.D., Penteado, H.L.D.B., Coutinho, L.F.C., Mendonca, F.J.G., 2015. Evaluation of the petroleum composition and quality with increasing thermal maturity as simulated by hydrous pyrolysis: A case study using a Brazilian source rock with Type I kerogen. Org. Geochem. 83–84, 27–53.

Stanley, S.M., Yang, X., 1994. A double mass extinction at the end of the Paleozoic era. Science 266, 1340–1344.

Svensen, H., Planke, S., Polozov, A.G., Schmidbauer, N., Corfu, F., Podladchikov, Y.Y., Jamtveit, B.R., 2009. Siberian gas venting and the end-Permian environmental crisis. Earth Planet. Sci. Lett. 277, 490–500.

Tetsuji, O., Naoto, T., Mitsutaka, M., Honami, S., Akira, I., Kasuhito, S., Yuji, S., Yukio, I., 2019. Enhanced flux of extraterrestrial 3He across the Permian-Triassic boundary. Progr. Earth Planet. Sci. 6, 18.

Teichmüller, M., 1986. Organic petrology of source rocks, history and state of the art. Org. Geochem. 10, 581–599.

Tian, Y.J., 2013. Source Material Separation of Mesophase Spherule and Preparation and Application of Carbonaceous Mesophase. Ph.D. dissertation. China University of Mining and Technology (in Chinese with English abstract).

Vajda, V., McLoughlin, S., Mays, C., Frank, T., Fielding, C., Tevyaw, A., Lethsten, V., Bocking, M., Nicoll, R.S., 2020. End-Permian (252 Mya) deforestation, wildfires and flooding—An ancient biotic crisis with lessons for the present. Earth Planet. Sci. Lett. 529, 115875.

Waples, D.W., 2000. The kinetics of in-reservoir oil destruction and gas formation: constraints from experimental and empirical data, and from thermodynamics. Org. Geochem. 31, 553–575.

Warren, J., 2000. Dolomite: occurrence, evolution and economically important associations. Earth-Sci. Rev. 52, 1–81.

Wei, G.Q., Shen, P., Yang, W., Zhang, J., Jiao, G.H., Xie, W.R., Xie, Z.Y., 2013. Formation conditions and exploration prospects of Sinian large gas fields, Sichuan Basin. Pet. Explor. Dev. 40, 139–149 (in Chinese with English abstract).

Wen, L., Li, Y., Yi, H.Y., Liu, X., Zhang, B.J., Qiu, Y.C., Zhou, G., Zhang, X.H., 2019. Lithofacies and reservoir characteristics of Permian volcanic rocks in the Sichuan Basin. Nat. Gas Ind. 39, 17–27 (in Chinese with English abstract).

White, J.L., 1976. Mesophase mechanisms in the formation of the microstructure of petroleum coke. Petroleum-derived Carbons 21, 282–314.

White, J.L., Price, R.J., 1974. The formation of mesophase microstructures during the pyrolysis of selected coker feedstocks. Carbon 12 (3), 321–333.

Wignall, P.B., 2001. Large igneous provinces and mass extinctions. Earth-Sci. Rev. 53, 1–33.

Wignall, P.B., Sun, Y.D., Bond, D.P.G., Izon, G., Newton, R.J., Vedrine, S., Widdowson, M., Ali, J.R., Lai, X.L., Jiang, H.S., Cope, H., Bottrell, S.H., 2009. Volcanism, mass extinction, and carbon isotope fluctuations in the Middle Permian of China. Science 324 (5931), 1179–1182.

Xie, S.C., Pancost, R.D., Huang, J.H., Wignall, P.B., Yu, J.X., Tang, X.Y., Chen, L., Huang, X.Y., Lai, X.L., 2007. Changes in the global carbon cycle occurred as two episodes during the Permian-Triassic crisis. Geology 35, 1083.

Yang, C.Y., Ni, Z.Y., Li, M.J., Wang, T.G., Chen, Z.H., Hong, H.T., Tian, X.W., 2018a. Pyrobitumen in South China: Organic petrology, chemical composition and geological significance. Int. J. Coal Geol. 188, 51–63.

Yang, C.Y., Ni, Z.Y., Wang, T.G., Chen, Z.H., Hong, H.T., Wen, L., Luo, B., Wang, W.Z., 2018b. A new genetic mechanism of natural gas accumulation. Sci. Rep. 8, 8336.

Yang, P., Ding, B.Z., Fan, C., Zhu, X.H., Wang, Y.J., Yang, P., 2017. Distribution pattern and origin of the columnar pull-down anomalies in Gaoshiti Block of Central Sichuan Basin, SW China. Pet. Explor. Dev. 44, 370–379 (in Chinese with English abstract).

Yin, M.D., Li, W.B., Sun, X.W., 2009. Rb–Sr isotope dating of sphalerite from the giant Huize Zn-Pb ore field Yunnan Province, southwestern China. Chin. J. Geochem. 28, 70–75 (in Chinese with English abstract).

Zhang, F.F., Algeo, T.J., Romaniello, S.J., Cui, Y., Zhao, L.S., Chen, Z.Q., Anbar, A.D., 2018. Congruent Permian-Triassic δ238U records at Panthalassic and Tethyan sites: Confirmation of global-oceanic anoxia and validation of the U-isotope paleoredox proxy. Geology 46, 327–330.

Zhang, P.W., Liu, G.D.L., Cai, C.F., Li, M.J., Chen, R.Q., Gao, P., Xu, C.L., Wan, W.C., Zhang, Y.Y., Jiang, M.Y., 2019. Alteration of solid bitumen by hydrothermal heating and thermochemical sulfate reduction in the Ediacaran and Cambrian dolomite reservoirs in the Central Sichuan Basin. SW China. Precambrian Res. 321, 277–302.

Zhong, Y.T., He, B., Mundil, R., Xu, Y.G., 2014. CA-TIMS zircon U-Pb dating of felsic ignimbrite from the Binchuan section: Implications for the termination age of Emeishan large igneous province. Lithos 204, 14–19.

Zhu, C.Q., Hu, S.B., Qiu, N.S., Rao, S., Yuan, Y.S., 2016. The thermal history of the Sichuan Basin, SW China: Evidence from the deep boreholes. Sci. China: Earth Sci. 59, 70–82.

Zhu, G.Y., Wang, T.S., Xie, Z.Y., Xie, B.H., Liu, K.Y., 2015. Giant gas discovery in the Precambrian deeply buried reservoirs in the Sichuan Basin, China: Implications for gas exploration in old cratonic basins. Precambrian Res. 262, 45–66.

Zou, C.N., Du, J.H., Xu, C.C., Wang, Z.C., Zhang, B.M., Wei, G.Q., Wang, T.S., Yao, G.S., Deng, S.H., Liu, J.L., 2014. Formation, distribution, resource potential, and discovery of Sinian-Cambrian giant gas field, Sichuan Basin, SW China. Pet. Explor. Dev. 41, 306–325 (in Chinese with English abstract).